Pulse shaping by difference-frequency mixing with quasi-phase-matching gratings

G. Imeshev and M. M. Fejer

E. L. Ginzton Laboratory, Stanford University, Stanford, California 94305

A. Galvanauskas and D. Harter

IMRA America, 1044 Woodridge Avenue, Ann Arbor, Michigan 48105

Received July 10, 2000; revised manuscript received October 9, 2000

We present a theory of ultrashort-pulse difference-frequency generation (DFG) with quasi-phase-matching (QPM) gratings in the undepleted-pump, unamplified-signal approximation. In the special case of a cw (or quasi-cw) pump, the spectrum of the generated idler is related to the spectrum of the signal through a transfer-function relation that is valid for arbitrary dispersion in the medium. The engineerability of this QPM-DFG transfer function establishes the basis for arbitrary pulse shaping. Experimentally we demonstrate QPM-DFG devices operating in a frequency-degenerate type II configuration and producing pulse-shaped output at 1550 nm from 220-fs pulses at 1550 nm. © 2001 Optical Society of America

OCIS codes: 140.7090, 190.7110, 190.2620, 190.4360, 230.4320, 320.5540, 320.7110, 320.7080.

1. INTRODUCTION

For many applications it is necessary to modify the temporal shape of ultrashort optical pulses obtained from a laser source in a well-defined manner.[1] The utility of longitudinally nonuniform quasi-phase-matching (QPM) gratings for pulse compression and shaping by the second-harmonic generation (SHG) process has been demonstrated.[2–9] This technique relies on the engineerability of the QPM gratings and allows shaping of pulses at half the wavelength of the seed pulses. This substantial wavelength shift, inherent to SHG, could be disadvantageous for certain applications, such as for fiber-optic communication systems at 1550 nm. Also, if it is desirable to obtain shaped pulses at a wavelength other than the harmonic of the seed, the SHG process does not provide adequate flexibility.

In this paper we present a theory of difference-frequency generation (DFG) with longitudinally nonuniform QPM gratings. Under the assumptions of plane waves, an undepleted pump, an unamplified signal, slowly varying amplitudes, and a cw pump wave, we derive a transfer-function relation between spectra of the seed signal and the shaped idler, valid for arbitrary material dispersion and pulse shapes. Similar to the QPM-SHG transfer function, this QPM-DFG transfer function can be engineered by controlling the duty cycle and the k-vector distribution of the grating, hence serving as a basis for fairly arbitrary pulse shaping. The advantage of the QPM-DFG shaping over the QPM-SHG shaping is that, by use of the former, the idler can be produced at any wavelength that can be phase matched by QPM. Also, in the QPM-DFG shaping case the shaped-pulse spectrum is linear in the seed-pulse spectrum, making straightforward the accounting of the group-velocity dispersion (GVD) and higher-order dispersion terms in the design of the shaper, whereas such accounting in the QPM-SHG case is complicated.[9]

As an example of this technique, we experimentally demonstrate QPM-DFG pulse-shaping devices operating in the type II phase-matching configuration, which allows shaped idler pulses to be obtained at the same wavelength, 1550 nm, as the seed signal pulses.

2. THEORY

The theoretical treatment of the QPM-DFG process with longitudinally nonuniform gratings presented in this paper is similar to that used for the analysis of the QPM-SHG process in Refs. 8 and 9. We assume plane-wave interactions along the propagation direction z in a lossless, nongyrotropic medium of length L. We consider the process of idler generation from the input signal and pump waves in the undepleted-pump and unamplified-signal approximation. Starting from the Maxwell's equations in the frequency domain, we arrive at the following set of coupled one-dimensional frequency-domain scalar wave equations:

$$\frac{\partial^2}{\partial z^2}\hat{E}_i(z,\omega) + k^2(\omega)\hat{E}_i(z,\omega) = -\mu_0\omega^2\hat{P}_{\mathrm{NL}}(z,\omega), \quad (1)$$

$$\frac{\partial^2}{\partial z^2}\hat{E}_s(z,\omega) + k^2(\omega)\hat{E}_s(z,\omega) = 0, \quad (2)$$

$$\frac{\partial^2}{\partial z^2}\hat{E}_p(z,\omega) + k^2(\omega)\hat{E}_p(z,\omega) = 0, \quad (3)$$

where $\hat{E}_m(z,\omega)$ is the Fourier transform of the electric field; here, and in the rest of the paper, a hat denotes the Fourier transform and subscript $m = i,\ s,\ p$ denotes the idler, signal, and pump, respectively. In Eqs. (1)–(3),

$k(\omega)$ is the frequency-dependent k vector, and $k(\omega) = (\omega/c)n(\omega)$, where $n(\omega)$ is the refractive index.

In a medium whose nonlinear coefficient is negligibly dispersive, the nonlinear polarization spectrum, $\hat{P}_{\mathrm{NL}}(z, \omega)$, which drives the idler generation, can be written in terms of the signal and pump electric fields in the form[10]

$$\hat{P}_{\mathrm{NL}}(z, \omega) = 2\varepsilon_0 d(z) \int_{-\infty}^{+\infty} \widehat{E_s^*}(z, \omega - \omega')\hat{E}_p(z, \omega')\mathrm{d}\omega', \tag{4}$$

where $d(z)$ is the material nonlinear coefficient, allowed here to vary with position to describe the modulation that is due to the presence of the QPM grating.

As in Ref. 8, we use the frequency-domain envelopes $\hat{A}_m(z, \Omega_m)$, defined by

$$\hat{E}_m(z, \omega) = \hat{A}_m(z, \Omega_m)\exp[-ik(\omega_m + \Omega_m)z], \tag{5}$$

where the k vector is a function of frequency and we introduce the frequency detunings $\Omega_m = \omega - \omega_m$ from the optical carrier angular frequency ω_m. This definition explicitly accounts for the effect of material dispersion on each frequency component of the interacting waves. These envelopes should not be confused with the conventional envelopes $B_m(z, t)$, defined in the time domain, such that the Fourier transform of the electric field is expressed as

$$\hat{E}_m(z, \omega) = \hat{B}_m(z, \Omega_m)\exp[-ik(\omega_m)z], \tag{6}$$

with the k vector evaluated at the carrier frequency of the pulse. A more complete discussion of the envelopes is presented in Ref. 8.

In terms of these frequency-domain envelopes the coupled wave equations (1)–(3) can be rewritten as

$$\frac{\partial}{\partial z}\hat{A}_i(z, \Omega_i) = -i\frac{\mu_0\omega_i^2}{2k_i}\hat{P}_{\mathrm{NL}}(z, \Omega_i)\exp[ik(\omega_i + \Omega_i)z], \tag{7}$$

$$\frac{\partial}{\partial z}\hat{A}_s(z, \Omega_s) = 0, \tag{8}$$

$$\frac{\partial}{\partial z}\hat{A}_p(z, \Omega_p) = 0, \tag{9}$$

where we use the slowly varying envelope approximation, $\partial^2\hat{A}_m/\partial z^2 \ll k(\omega)(\partial\hat{A}_m/\partial z)$. The nonlinear polarization $\hat{P}_{\mathrm{NL}}(z, \Omega_i)$ is expressed with Eqs. (4) and (5) in terms of the signal and pump envelopes as

$$\hat{P}_{\mathrm{NL}}(z, \Omega) = 2\varepsilon_0 d(z) \int_{-\infty}^{+\infty} \widehat{A_s^*}(z, -\Omega + \Omega')\hat{A}_p(z, \Omega') \times \exp\{i[k(\omega_s - \Omega + \Omega') - k(\omega_p + \Omega')]z\}\mathrm{d}\Omega', \tag{10}$$

where we define $\Omega \equiv \Omega_i = \omega - \omega_i$, $\Omega' \equiv \omega' - \omega_p$, and use $\widehat{A_s^*}(-\Omega) = \widehat{A_s^*}(\Omega)$.

Equations (8) and (9) describe free propagation of the signal and pump waves through the dispersive medium; their solutions are

$$\hat{A}_s(z, \Omega) = \hat{A}_s(\Omega), \tag{11}$$

$$\hat{A}_p(z, \Omega) = \hat{A}_p(\Omega), \tag{12}$$

where $\hat{A}_s(\Omega) = \hat{A}_s(z = 0, \Omega)$ is the signal envelope and $\hat{A}_p(\Omega) = \hat{A}_p(z = 0, \Omega)$ is the pump envelope at the input ($z = 0$) of the nonlinear crystal.

Substituting the solutions (11) and (12) into the expression for $\hat{P}_{\mathrm{NL}}(z, \Omega)$, Eq. (10), we obtain the output idler envelope by integrating Eq. (7):

$$\hat{A}_i(L, \Omega) = -i\gamma\int_0^L d(z)\mathrm{d}z \int_{-\infty}^{+\infty} d\Omega'\hat{A}_s^*(\Omega' - \Omega) \times \hat{A}_p(\Omega')\exp[-i\Delta k(\Omega, \Omega')z], \tag{13}$$

where $\gamma \equiv 2\pi/(\lambda_i n_i)$, λ_i is the idler wavelength, and n_i is the refractive index at the idler frequency and the k-vector mismatch

$$\Delta k(\Omega, \Omega') = k(\omega_p + \Omega') - k(\omega_i + \Omega) - k(\omega_s + \Omega' - \Omega). \tag{14}$$

With Eqs. (13) and (14) one can find the output idler envelope $\hat{A}_i$, given the following: the input signal and pump envelopes $\hat{A}_s$ and $\hat{A}_p$, respectively, the dispersive properties of the medium, represented by the functional dependence $\Delta k = \Delta k(\Omega, \Omega')$, and the modulated nonlinear coefficient $d(z)$. We note that Eq. (13) is valid for materials with arbitrary dispersion or, equivalently, for interacting pulses with arbitrarily broad spectra.

Now we assume that the pump is a cw monochromatic wave, i.e., its frequency-domain envelope is a delta function,

$$\hat{A}_p(\Omega) = E_p\delta(\Omega = 0), \tag{15}$$

where E_p is the amplitude of the pump wave. Substituting Eq. (15) into Eq. (13) we obtain

$$\hat{A}_i(L, \Omega) = \hat{d}(\Omega)\hat{A}_s^*(-\Omega)E_p, \tag{16}$$

where $\hat{d}(\Omega)$ is proportional to the spatial Fourier transform of $d(z)$,

$$\hat{d}(\Omega) = -i\gamma\int_{-\infty}^{+\infty} d(z)\exp[-i\Delta k(\Omega)z]\mathrm{d}z, \tag{17}$$

where $\Delta k(\Omega)$ serves as the transform variable and is defined as

$$\Delta k(\Omega) = k(\omega_p) - k(\omega_i + \Omega) - k(\omega_s - \Omega). \tag{18}$$

In Eq. (17) we extended the limits of integration from $[0, L]$ to $(-\infty, +\infty)$ realizing that this cannot affect the solution since $d(z) = 0$ outside of the crystal.

The result of Eq. (16) can be rewritten in terms of the Fourier transform of the conventional time-domain envelopes as

$$\hat{B}_i(L, \Omega) = \hat{d}(\Omega)\hat{B}_s^*(-\Omega)E_p\exp\{-i[k(\omega_i + \Omega) - k(\omega_i)]L\}. \tag{19}$$

It is interesting to note that when $\hat{d}(\Omega)$ is essentially constant over the bandwidth of the signal pulse, Eq. (16) de-

scribes the effect of spectral inversion of the spectrum of the idler relative to the spectrum of the signal.

Assuming $\Omega \ll \omega_i, \omega_s$, we perform a Taylor expansion in Eq. (18), resulting in

$$\Delta k(\Omega) = \Delta k_0 + \delta\nu_{si}\Omega - \sum_{n=2}^{\infty} \frac{1}{n!}[(-1)^n \beta_{sn} + \beta_{in}]\Omega^n, \tag{20}$$

where $\Delta k_0 = k(\omega_p) - k(\omega_s) - k(\omega_i)$ is the carrier k-vector mismatch, $\delta\nu_{si} = 1/u_s - 1/u_i$ is the signal–idler group-velocity mismatch (GVM) parameter, where $u_m = [\mathrm{d}k(\omega)/\mathrm{d}\omega]^{-1}|_{\omega=\omega_m}$ are the group velocities, and $\beta_{mn} = [\mathrm{d}^n k(\omega)/\mathrm{d}\omega^n]|_{\omega=\omega_m}$ are the GVD ($n = 2$), third-order dispersion ($n = 3$), etc., coefficients. The characteristic lengths at which a particular dispersive term becomes important for a transform-limited pulse of length τ_0 is $L_{\beta mn} = \tau_0^n/|\beta_{mn}|$. In the case when GVD and higher-order dispersion terms can be neglected, i.e., when $L \ll L_{\beta mn}$ for all m (all interacting waves) and all $n \geqslant 2$ (all dispersive terms beyond GVM), Eq. (17) becomes

$$\hat{d}(\Omega) = -i\gamma \int_{-\infty}^{+\infty} d(z)\exp[-i(\Delta k_0 + \delta\nu_{si}\Omega)z]\mathrm{d}z, \tag{21}$$

which has the same form as the QPM-SHG transfer function derived neglecting dispersion beyond GVM.[2,8]

In Eq. (16) the factor $\hat{d}(\Omega)$ is a transfer function that relates the spectrum of the idler to the spectrum of the signal. $\hat{d}(\Omega)$ depends only on the dispersive properties of the medium and the modulated nonlinear coefficient distribution, but not on any of the input-pulse parameters, and hence can be viewed as a filter function acting on the different spectral components of the signal pulse. This transfer-function result is the basis for fairly general pulse shaping with QPM gratings. Given the input signal pulse and the desired shaped idler pulse, the necessary transfer function is obtained from Eq. (16) simply as $\hat{d}(\Omega) \propto \hat{A}_i(L, \Omega)/\hat{A}_s^*(-\Omega)$, from which the desired distribution of the nonlinear coefficient $d(z)$ is obtained from Eq. (17) with the inverse Fourier transform. Since $d(z)$ can be engineered by controlling the local duty cycle and the local QPM period distribution of the grating,[4,8] an idler pulse of any desired shape can be obtained from a given signal pulse. For example, a linearly chirped QPM grating[2,8] can be used to generate compressed idler pulses from linearly chirped signal pulses.

The QPM-DFG transfer-function relation, Eq. (16), is very similar to the QPM-SHG transfer function.[2,8,9] The important difference, however, is that in the SHG case the spectrum of the shaped second harmonic, $\hat{A}_2(L, \Omega)$, is linearly related to the spectrum of the *square* of the first harmonic (FH), $\widehat{A_1^2}(\Omega)$ (Refs. 2, 8, and 9):

$$\hat{A}_2(L, \Omega) = \hat{D}(\Omega)\widehat{A_1^2}(\Omega), \tag{22}$$

where $\hat{D}(\Omega)$ is the QPM-SHG transfer function. In contrast, the QPM-DFG transfer-function result, Eq. (16), has the form of a linear filter in the frequency domain, relating the spectrum of the shaped idler to the spectrum of the seed signal. This distinction has a profound effect on how GVD and higher-order dispersion of the nonlinear medium can be accounted for in the design of the shaper.

In deriving the QPM-SHG transfer-function relation, Eq. (22), we had to assume that GVD and higher-order dispersion terms at the FH could be neglected, resulting in the following expression for the QPM-SHG transfer function $\hat{D}(\Omega)$ (Refs. 2, 8, and 9):

$$\hat{D}(\Omega) = -i\gamma \int_{-\infty}^{+\infty} d(z)\exp[-i\Delta k(\Omega)z]\mathrm{d}z, \tag{23}$$

where $\Delta k(\Omega)$ is the k vector mismatch for the SHG process. If GVD and higher-order dispersion at the FH are nonnegligible and included in the analysis, the expression for $\hat{A}_2(L, \Omega)$ has an integral form,[8,9] more complicated than a transfer-function result of Eq. (22), which did not provide a ready way for the design of $d(z)$ necessary for a particular shaping function. Accounting for GVD and higher-order dispersion at the FH in the design of a pulse shaper is relatively complicated; the appropriate design procedures were described in Ref. 9. On the contrary, in the QPM-DFG case with a cw pump, the simple transfer-function relation, Eq. (16), holds for arbitrary dispersion at all the interacting wavelengths, as can be seen from Eq. (18) or Eq. (20).

We note that Eq. (16) still holds if instead of a cw monochromatic pump, which has a delta-function spectrum, a pump wave with a sufficiently narrow spectrum is used. In the time domain it corresponds to a long, compared with the signal, pulse. More precisely, the pump pulse length τ_p should be longer than the pump–signal group delay accumulated in the crystal of a given length, $\tau_p > |\delta\nu_{sp}|L$, where $\delta\nu_{sp} = 1/u_s - 1/u_p$ is the pump–signal GVM parameter.

In the time domain the QPM-DFG pulse shaping relies on a combination of two effects: spatial localization of conversion and GVM between signal and idler pulses. A particular frequency component of the signal mixes with the pump to generate a corresponding idler frequency component at spatial positions where the DFG process is phase matched. Because of the GVM, this idler frequency component undergoes a particular time delay relative to the signal pulse, as observed at the output of the grating. This time delay is determined by the GVM parameter $\delta\nu_{si}$ and the spatial position at which the idler is generated, the former being a material property, whereas the latter is defined by the grating design. This time-domain picture can be derived from the definition of the QPM-DFG transfer function, Eq. (21), which states that for every frequency Ω, $\hat{d}(\Omega)$ is obtained by summing contributions from different sections of the QPM grating, with phase delays determined by the longitudinal coordinate z and the GVM parameter $\delta\nu_{si}$.

The maximum possible temporal window T (or the best spectral resolution $\delta\Omega \propto 1/T$) of the shaper is determined by the length L of the device, $T = \delta\nu_{si}L$. We note that the transfer-function relation, Eq. (16), predicts the shaped idler spectrum but in principle does not set the limit on the bandwidth of the generated idler. However, since the QPM grating acts as a passive filter, not as an amplifier, the bandwidth of the idler pulse cannot exceed the bandwidth of the seed signal, at least not without pay-

ing the price of significant efficiency reduction. Therefore the shortest temporal feature of the shaped idler that can be obtained, δt, is inversely related to the bandwidth, $\Delta\Omega_s$, available from the seed signal pulse, $\delta t \propto 1/\Delta\Omega_s$, with the proportionality constant being of the order of unity and its exact value depending on the shape of the pulses.

The efficiency of a QPM-DFG shaper is a complicated function of focusing, spectra of the pulses, and the particular shaping function used. For particular specific cases it can be analyzed in the same manner as was presented in Ref. 8 for the QPM-SHG shaping case. For example, we calculate the idler pulse energy in the case in which the acceptance bandwidth of the QPM-DFG shaper, $\Delta\Omega_g$, is much narrower than the bandwidth of the signal pulse $\Delta\Omega_s$, i.e., $\Delta\Omega_g \ll \Delta\Omega_s$. We assume that a Gaussian signal pulse with full width at half-maximum (FWHM) of τ_s is mixed with a top-hat pump pulse with pulse length τ_p. We use the result of Eq. (15) and integrate the idler spectral intensity over all frequencies; assuming optimum focusing,[11] i.e., the pump and the signal have equal confocal parameters chosen to generate a confocally focused idler, the idler pulse energy is then obtained as

$$U_i = \frac{538}{c\varepsilon_0}\frac{|d|}{n^2\delta\nu_{si}}\frac{(\lambda_s - \lambda_p)^3}{(\lambda_s + \lambda_p)^2\lambda_s^2\lambda_p^2}\frac{\tau_s}{\tau_p} f U_s U_p, \qquad (24)$$

where f is the grating fill factor, and $|d|$ is related to the intrinsic material nonlinearity d_{eff} as $|d| = (2/\pi)d_{\text{eff}}$ for first-order QPM. For pump wavelength 780 nm, signal wavelength 1.56 μm, and a QPM-DFG shaper on a lithium niobate substrate operating in the type II configuration to produce an orthogonally polarized shaped idler pulse at the wavelength of 1.56 μm, the idler pulse energy is obtained with Eq. (24) as $U_i = 7.2\%/\text{nJ}\ (\tau_s/\tau_p) f U_s U_p$. In comparison, the efficiency for the QPM-SHG shaper pumped at 1.56 μm was obtained in Ref. 8 as $U_2 = 265\%/\text{nJ}\ f U_1^2$. As can be seen, the QPM-DFG shaper suffers considerable efficiency reduction compared with the QPM-SHG shaper. The first reason for this efficiency reduction is intrinsic to the QPM-DFG case τ_s/τ_p factor. The second is because the QPM-DFG shaper considered operates in the wavelength-degenerate type II configuration and hence uses lower nonlinearity ($d_{\text{eff}} = d_{31} = 4.3$ pm/V, Ref. 12) compared with the QPM-SHG shaper ($d_{\text{eff}} = d_{33} = 27$ pm/V, Ref. 12). For a wavelength nondegenerate case, type I DFG configuration ($d_{\text{eff}} = d_{33}$) can be used, resulting in a higher efficiency: $U_i = 140\%/\text{nJ}\ (\tau_s/\tau_p) f U_s U_p$, where we assumed a pump wave at 532 nm, a short signal pulse at 800 nm, and a shaped idler at 1.59 μm.

We note that the analysis presented in this paper for a particular QPM-DFG case, i.e., using a (quasi-) cw pump wave, using a signal wave as a seed, and obtaining shaped pulses at the idler wavelength, can be trivially modified to describe any three-wave mixing process with one of the waves (the seed pulse) mixed with the second wave (a cw or quasi-cw wave) to generate a shaped pulse, provided that the two input fields are undepleted or unamplified. For example, the theory presented describes a single-pass idler generation process in a synchronously pumped optical parametric oscillator assuming a low single-pass gain, short pump pulse, and a narrow-band resonated signal pulse (which can be achieved by inserting a bandpass filter in the optical parametric oscillator cavity). On the other hand, these assumptions are violated in the case of a high-gain optical parametric generation process; the presented theory cannot be applied in that case.

3. EXPERIMENT

Using QPM to achieve phase matching in a type II configuration was proposed previously[13] and demonstrated recently in periodically poled KTP.[14] The advantage of the type II configuration for QPM-DFG pulse shaping is that it allows shaping of idler pulses at the same wavelength as the seed signal pulses, but with orthogonal polarization. For a pump at a wavelength of 775 nm and a signal at a wavelength of 1.55 μm the GVM coefficient $\delta\nu_{si} = 0.26$ ps/mm between orthogonally polarized signal and idler is large enough to achieve the necessary group delay in a device tens of millimeters long.

Here we describe an experiment with degenerate type II DFG, pumped by a long top-hat pulse at 775 nm (Fig. 1). The pump laser was an amplified Er:fiber laser producing 90-nJ, 600-fs pulses at 1.55 μm. The output of this source was split into two arms.

In the first arm we generated the pump pulse for the QPM-DFG shaper by SHG in a periodically poled lithium niobate crystal whose length, 25 mm, was longer than the walk-off length, 2.0 mm, between the fundamental and the second harmonic (SH). The resulting SH pulse had a top-hat shape and a length of $\tau_p = 7.4$ ps, which was longer than the group delay of 6.8 ps between this pulse and the seed signal pulse, accumulated in the shaper chip of $L = 20$ mm. The grating had a period of 168.75 μm and was held at 118 °C to achieve 9th-QPM-order generation. The SH pulses had an energy of 6 nJ per pulse. To generate this long pulse with a fairly flat intensity profile in a simple uniform grating, the efficiency had to be kept $<10\%$. Consequently, a higher QPM order was used to avoid overdriving the nonlinear process in the long crystal of limited transverse aperture.

In the second arm, pulses from the amplified Er:fiber laser were self-phase-modulated in a 50-cm-long fiber with dispersion $\beta_2 = +108\ \text{ps}^2/\text{m}$. The output pulses of 14-nm bandwidth were compressed to $\tau_s = 220$ fs in a grating compressor. The resulting signal pulses had an energy of 5 nJ.

The pump and the signal beams (both polarized as ordinary waves) were recombined and focused through the QPM-DFG shaper into spot sizes of 43 and 63 μm, respectively. The shaped idler pulses (extraordinary wave) were separated from the seed signal pulses with a polar-

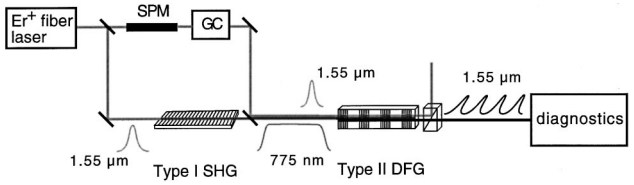

Fig. 1. Experimental setup. SPM is the self-phase-modulating fiber and GC is the grating compressor.

izing beam splitter and then amplified in a zero-dispersion fiber amplifier for temporal characterization with an autocorrelator.

As examples of QPM-DFG shapers, we fabricated three devices [henceforth labeled as (a), (b), and (c)] of length 20 mm on a single chip by electric-field poling of a lithium niobate wafer.[13] To achieve phase matching for type II DFG, the QPM period of the shaper was selected to be 9.45 μm and the chip was held at 134 °C. The GVD parameters for signal and idler are calculated by use of published Sellmeier data for the ordinary wave[15] and the extraordinary wave[16] as $\beta_{2s} = 112\,\mathrm{fs}^2/\mathrm{mm}$ and $\beta_{2i} = 103\,\mathrm{fs}^2/\mathrm{mm}$, respectively. The crystal length at which GVD starts to play a significant role for 220-fs pulses is $L_{\beta 2} = 45\,\mathrm{cm}$, which is substantially longer than the length $L = 20\,\mathrm{mm}$ of the QPM-DFG shapers used in the experiment. Hence no compensation for GVD and higher-order dispersion was necessary in the design of the shapers, and the simplified version of the transfer function, Eq. (21), was used for the analysis.

Device (a) was simply a uniform grating whose length of 20 mm was much longer than the signal–idler walk-off length $L_{\mathrm{gv}} = \tau_s/\delta\nu_{si} = 0.85\,\mathrm{mm}$. The idler-pulse autocorrelation trace [Fig. 2(a)] has a triangular profile which implies a top-hat pulse. The FWHM of the trace (and the pulse) is 5.1 ps, in agreement with the expected value of $\delta\nu_{si}L = 5.2\,\mathrm{ps}$. The generated shaped idler pulse had an energy of 10 pJ, which gives lower than the ideal efficiency (see Section 2) mainly because the focusing used in experiment was not optimal.

Device (b) had six uniform grating segments of length 0.6 mm, alternating with 2.9-mm-long segments of unmodulated material, where conversion was negligible. Each grating segment generated a short pulse, since its length was shorter than L_{gv}. Because of the group-velocity walk-off effect, these pulses did not overlap at the output. The idler autocorrelation trace [Fig. 2(b)] consists of eleven pulses separated by $\Delta T = 0.90\,\mathrm{ps}$ and has a triangular envelope. Thus the pulse waveform has six pulses of equal amplitudes. The length of an individual pulse is estimated from the trace as ~200 fs. The shaped pulse had an energy of 1.2 pJ.

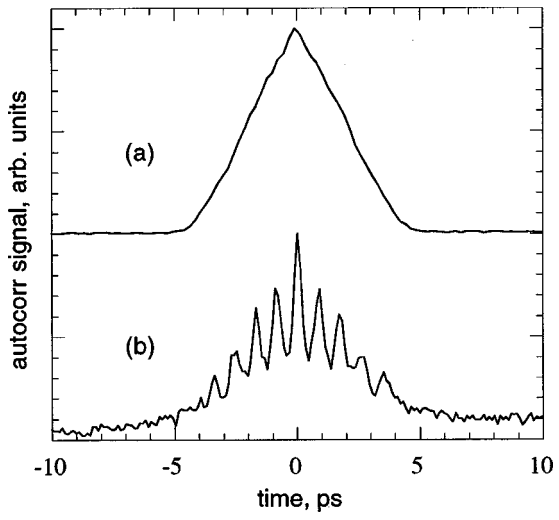

Fig. 2. Autocorrelation traces of the shaped idler pulses: long top-hat picosecond pulse, trace (a); train of six pulses of length of approximately 200 fs, trace (b). Note that for clarity the traces are offset vertically with respect to each other.

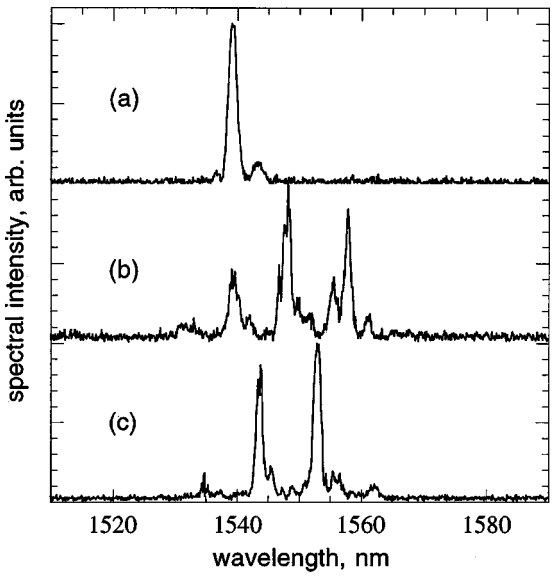

Fig. 3. Spectra of shaped idler pulses obtained with devices (a), (b), and (c).

Device (c) was essentially identical to device (b) except that alternate grating segments were shifted by exactly one coherence length (half the QPM period) to generate idler pulses with alternating phases. Because the intensity autocorrelation loses phase information, the autocorrelation trace for this device (not shown) was identical to that of device (b). The difference between the pulse trains produced by devices (b) and (c) is revealed in the pulse spectra.

Figure 3 shows the spectra of the shaped idler pulses. Device (a) produced a single narrow spectral peak, consistent with a generated long pulse. Device (b) shows a series of spectral peaks, as expected for a train of coherent pulses. The peak separation is determined by the temporal separation between the pulses, $\Delta\Omega = 1/\Delta T$, whereas the number of peaks is determined by the ratio of a single pulse bandwidth to the peak separation. The observed wavelength separation of ~9 nm agrees with the expected value $\Delta\Omega = 1.1\,\mathrm{ps}^{-1}$. Device (c) can be viewed as obtained from device (b) by superimposing a phase-reversal sequence with a period twice the separation between the grating segments. In the frequency domain this modulation leads to each spectral peak splitting into two peaks shifted by $\Delta\Omega/2$ with respect to the original peak, which is exactly what we see by comparing spectra (b) and (c). The slight wavelength shift of the spectrum of device (a) relative to the spectra of devices (b) and (c) is because the spectrum of the long pump pulse was not at exactly half the wavelength of the seed pulse.

4. CONCLUSIONS

In conclusion, we demonstrated a new pulse-shaping technique based on DFG with Fourier synthetic QPM gratings. Clearly, this method can be extended to any three-wave mixing processes such as mid-infrared DFG, ultraviolet, and visible sum-frequency generation. Also

shaping functions such as pulse compression and matched filtering, and others such as have been demonstrated with conventional shaping techniques,[1] are possible.

ACKNOWLEDGMENTS

We thank Crystal Technology for a generous donation of lithium niobate wafers. This research was supported by U.S. Air Force Office of Scientific Research grant F49620-99-1-0270. G. Imeshev acknowledges support from IMRA America.

M. M. Fejer can be reached by e-mail at fejer@stanford.edu.

REFERENCES

1. A. M. Weiner, "Femtosecond optical pulse shaping and processing," Prog. Quantum Electron. **19**, 161–237 (1995).
2. M. A. Arbore, O. Marco, and M. M. Fejer, "Pulse compression during second-harmonic generation in aperiodic quasi-phase-matching gratings," Opt. Lett. **22**, 865–867 (1997).
3. M. A. Arbore, A. Galvanauskas, D. Harter, M. H. Chou, and M. M. Fejer, "Engineerable compression of ultrashort pulses by use of second-harmonic generation in chirped-period-poled lithium niobate," Opt. Lett. **22**, 1341–1343 (1997).
4. G. Imeshev, A. Galvanauskas, D. Harter, M. A. Arbore, M. Proctor, and M. M. Fejer, "Engineerable femtosecond pulse shaping by second-harmonic generation with Fourier synthetic quasi-phase-matching gratings," Opt. Lett. **23**, 864–866 (1998).
5. M. Hofer, M. E. Fermann, A. Galvanauskas, D. Harter, and R. S. Windeler, "Low-noise amplification of high-power pulses in multimode fibers," IEEE Photonics Technol. Lett. **11**, 650–652 (1999).
6. P. Loza-Alvarez, D. T. Reid, P. Faller, M. Ebrahimzadeh, and W. Sibbett, "Simultaneous second-harmonic generation and femtosecond-pulse compression in aperiodically poled $KTiOPO_4$ with a $RbTiOAsO_4$-based optical parametric oscillator," J. Opt. Soc. Am. B **16**, 1553–1560 (1999).
7. P. Loza-Alvarez, D. T. Reid, P. Faller, M. Ebrahimzadeh, W. Sibbett, H. Karlsson, and F. Laurell, "Simultaneous femtosecond-pulse compression and second-harmonic generation in aperiodically poled $KTiOPO_4$," Opt. Lett. **24**, 1071–1073 (1999).
8. G. Imeshev, M. A. Arbore, M. M. Fejer, A. Galvanauskas, M. Fermann, and D. Harter, "Ultrashort-pulse second-harmonic generation with longitudinally nonuniform quasi-phase-matching gratings: pulse compression and shaping," J. Opt. Soc. Am. B **17**, 304–318 (2000).
9. G. Imeshev, M. A. Arbore, S. Kasriel, and M. M. Fejer, "Pulse shaping and compression by second-harmonic generation with quasi-phase-matching gratings in the presence of arbitrary dispersion," J. Opt. Soc. Am. B **17**, 1420–1437 (2000).
10. S. K. Kurtz, in *Quantum Electronics: A Treatise*, H. Rabin and C. L. Tang, eds. (Academic, New York, 1975).
11. J.-J. Zondy, "The effects of focusing in type-I and type-II difference-frequency generations," Opt. Commun. **149**, 181–206 (1998).
12. D. A. Roberts, "Simplified characterization of uniaxial and biaxial nonlinear optical crystals: a plea for standardization of nomenclature and conventions," IEEE J. Quantum Electron. **28**, 2057–2074 (1992).
13. L. E. Myers, R. C. Eckardt, M. M. Fejer, R. L. Byer, W. R. Bosenberg, and J. W. Pierce, "Quasi-phase-matched optical parametric oscillators in bulk periodically poled $LiNbO_3$," J. Opt. Soc. Am. B **12**, 2102–2116 (1995).
14. S. Wang, V. Pasiskevicius, J. Hellström, F. Laurell, and H. Karlsson, "First-order type II quasi-phase-matched UV generation in periodically poled KTP," Opt. Lett. **24**, 978–980 (1999).
15. G. J. Edwards and M. Lawrence, "A temperature-dependent dispersion equation for congruently grown lithium niobate," Opt. Quantum Electron. **16**, 373–375 (1984).
16. D. H. Jundt, "Temperature-dependent Sellmeier equation for the index of refraction, n_e, in congruent lithium niobate," Opt. Lett. **22**, 1553–1555 (1997).